2826

19. C. P. McKay, S. C. Martin, C. A. Griffith, R. M. Keller *Icarus* **129**, 498 (1997).
20. J. R. Holton, *An Introduction to Dynamical Meteorology* (Academic Press, San Diego, CA, 1992).
21. E. Lellouch *et al.*, *Icarus* **79**, 328 (1989).
22. The LFC for supersaturated conditions in the mid to upper troposphere, as suggested by Courtin *et al.* (*27*) and Samuelson *et al.* (*28*), significantly exceeds those for saturated conditions. At 140% ambient supersaturation, the LFC lies at 13 km altitude for a parcel of 60% humidity starting at the surface.
23. M. Awal, J. L. Lunine, *Geophys. Res. Lett.* **21**, 2491 (1994).
24. The entrainment of local air breaks the conservation of θ_e for the rising plume. The increasing mass of a plume parcel, m, is parametrized as $\frac{1}{m}\frac{dm}{dz} = \frac{\alpha}{r}$ following laboratory simulations (*29*) in studies of clouds in Earth's tropics (*30*). Observations of terrestrial clouds indicate a value of $\alpha = 0.2$ and range of plume radii of $r = 0.6$ to 4 km.
25. The presence of rain agrees with the paucity of nucleation sites available in Titan's atmosphere (Table 1). In the terrestrial atmosphere, the initial size of a raindrop is roughly determined by the number of drops and the mass needed to lower a supersaturated atmosphere back to saturation. The existence of only a few nucleation sites brings about few cloud particles and large particle sizes. The only known source of nucleation sites on Titan is its haze, the number density of which is several orders of magnitude smaller than typical terrestrial values. Considering the low number density of nucleation sites compared to the high methane abundance, Toon *et al.* (*31*) realized that particles must grow to millimeter sizes to reduce several percent supersaturation to saturation conditions.
26. R. M. Goody, Y. L. Yung, *Atmospheric Radiation, Theoretical Basis* (Oxford Univ. Press, Oxford, 1989).
27. R. Courtin *et al.*, *Icarus* **114**, 144 (1995).
28. R. E. Samuelson *et al.*, *Planet. Space Sci.* **45**, 959 (1997).
29. H. Stommel, *J. Meteorol.* **4**, 91 (1947).
30. J. Simpson, G. W. Brier, R. H. Simpson, *J. Atmos. Sci.* **24**, 508 (1967).
31. O. B. Toon, C. P. McKay, R. Courtin, T. P. Ackerman, *Icarus* **75**, 255 (1988).
32. P. Gierasch, R. Goody, P. Stone, *Geophys. Fluid Dyn.* **1**, 1 (1970)
33. C.A.G. and J.L.H. are supported by the NASA Planetary Astronomy Program under grant NAG5-6790.

18 July 2000; accepted 21 September 2000

Acute Sensitivity of Landslide Rates to Initial Soil Porosity

R. M. Iverson,[1] M. E. Reid,[2] N. R. Iverson,[3] R. G. LaHusen,[1] M. Logan,[1] J. E. Mann,[3] D. L. Brien[2]

Some landslides move imperceptibly downslope, whereas others accelerate catastrophically. Experimental landslides triggered by rising pore water pressure moved at sharply contrasting rates due to small differences in initial porosity. Wet sandy soil with porosity of about 0.5 contracted during slope failure, partially liquefied, and accelerated within 1 second to speeds over 1 meter per second. The same soil with porosity of about 0.4 dilated during failure and slipped episodically at rates averaging 0.002 meter per second. Repeated slip episodes were induced by gradually rising pore water pressure and were arrested by pore dilation and attendant pore pressure decline.

In popular metaphor, landslide processes begin spontaneously and gain momentum as they proceed, but what determines how real landslides move? Can small differences in initial conditions cause some landslides to accelerate catastrophically and others to creep intermittently downslope? The distinction is important because rapid landslides pose lethal threats, whereas slow landslides damage property but seldom cause fatalities (*1*).

A longstanding hypothesis holds that landslide behavior may depend on initial soil porosity, because soils approach specific critical-state porosities during shear deformation (*2–4*). Tests on small soil specimens indicate that dense soils (initially less porous than critical) dilate as they begin to shear, whereas loose soils (initially more porous than critical) contract (*5–7*). Dilation can reduce pore water pressures and thereby retard continued deformation by increasing normal stresses and frictional strength at grain contacts, whereas contraction can increase pore water pressures and thereby reduce frictional strength (*8–10*). Positive feedback between frictional strength reduction and soil contraction may cause some landslides to transform into liquefied high-speed flows (*11–13*).

To isolate the effect of initial soil porosity on landslide style and rate, we conducted large-scale experiments under closely controlled conditions. In each of nine landslide experiments, we placed a 65-cm-thick, 6-m^3 rectangular prism of loamy sand soil (Table 1) on a planar concrete bed inclined 31° from horizontal and bounded laterally by vertical concrete walls 2 m apart (Fig. 1). The downslope end of each soil prism was restrained by a rigid wall, which ensured that deformation occurred at least partly within the soil mass (rather than along the bed) and that landsliding included a rotational component.

Different methods of soil placement yielded different initial porosities. The highest porosities (>0.5) were attained by dumping the soil in 0.5-m^3 loads and raking it into position, without otherwise touching its surface. Lower porosities resulted from placing the soil in 10-cm layers parallel to the bed and compacting each layer with either foot traffic or 16-Hz mechanical vibrations that delivered impulsive loads of ~2 kPa at depths of 10 cm (*14*). After placement of each soil prism, we determined porosities by excavating four to nine ~1-kg samples at various depths and measuring their volumes, masses, and water contents (*15*). No systematic variations of porosity with depth were detected.

Our suite of landslide experiments included individual tests with initial porosities ranging from 0.39 ± 0.03 to 0.55 ± 0.01 (±1 SD sampling error for an individual experiment). Ancillary tests of the same soil in a ring-shear device and triaxial cell produced dilative shear failure when initial porosity was ≤0.41 and contractive shear failure when initial porosity was ≥0.46 (Fig. 2 and Table 1). Landslides with initial porosities that bracketed the range from 0.41 to 0.46 were therefore of greatest interest.

Landslide motion was measured with two ground-surface extensometers and 17 or 18 subsurface tiltmeters arranged at depth increments of ~7 cm in two vertical nests (*16*). Pore water pressures were measured with 12 tensiometers and 12 dynamic piezometers arranged in three vertical nests at depth increments of ~20 cm (*17*) (Fig. 1). Data from each sensor were logged digitally at 20 Hz for the duration of each experiment.

To induce landsliding, soil prisms were watered with surface sprinklers and through subsurface channels that introduced simulated groundwater (Fig. 1). Rising water tables were kept nearly parallel to the impermeable bed by adjusting discharge from a drain at the base of the retaining wall. Although preliminary experiments indicated that different styles and rates of water application influenced the onset of slope failure, this influence became negligible as failure occurred and instigated changes in soil porosity (*18*, *19*).

Landslides with differing porosities displayed sharply contrasting dynamics (compare Figs. 3 and 4). Each of four landslides with initial porosities >0.5 failed abruptly and accelerated within 1 s to speeds >1 m/s. The surfaces of these landslides appeared fluid and smooth, and data from dynamic piezometers confirmed that pore water pressures rose rapidly during failure and reached levels nearly sufficient to balance total normal stresses and liquefy the soil (Fig. 3). Three landslides with

[1]U.S. Geological Survey, 5400 MacArthur Boulevard, Vancouver, WA 98661, USA. [2]U.S. Geological Survey, 345 Middlefield Road, Menlo Park, CA 94025, USA. [3]Department of Geological and Atmospheric Sciences, Iowa State University, Ames, IA 50011, USA.

initial porosities indistinguishable from the critical porosity (0.44 ± 0.03, 0.44 ± 0.03, and 0.42 ± 0.03) displayed inconsistent behavior, including slow slumping of a single soil block, episodic slumping of multiple blocks, and moderately rapid (~0.1 m/s) slumping that ceased after <0.5 m displacement. Dynamic piezometer data from these experiments revealed a complex mix of dilative and contractive soil behavior during failure. The landslide with the lowest and least variable initial porosity (0.41 ± 0.01) displayed the clearest dilative soil behavior as it underwent slow episodic motion (Fig. 4). Our attempt to induce a landslide with still lower porosity (0.39 ± 0.03) ended uneventfully because we could not impart pore water pressures sufficient to trigger slope failure (*20*).

Figure 3 illustrates how landsliding of loose soil (initial porosity 0.52 ± 0.02) can lead to rapid acceleration in the course of only 1 s. After about 2400 s of precursory sprinkling (with no groundwater inflow), positive pore water pressures developed first near the concrete bed and thereafter at shallower depths as a water table accreted vertically at rates ~0.05 cm/s. This wetting caused soil compaction, evidenced by a slight downslope rotation of tiltmeters at all depths, downslope surface displacement of nearly 10 cm, and vertical surface settlement of about 2 cm. As a consequence, average porosity declined to about 0.49, but the soil remained looser than critical. The soil developed no surface cracks or other visible signs of instability during this precursory period.

Failure of the loose soil began at about 2781 s (Fig. 3), when tiltmeters at all depths began to rotate slightly upslope and pore water pressure heads below the water table (at depths of 50 and 67 cm) began to rise at rates >10 cm/s as a result of soil contraction. Visible slope rupture commenced about 0.5 s later (2781.5 s in Fig. 3), accompanied by rapidly accelerating surface displacement, divergence of tilts at different depths, and continuing pressure-head rise. In about 1 s, pressure heads at 30-cm depth increased from zero (atmospheric) values to hydrostatic values (~30 cm) as soil contraction forced the water table upward. Even larger increases in pressure heads at depths of 50 and 67 cm indicated that an upward head gradient developed, which promoted soil liquefaction. By 2783 s (Fig. 3), pore water pressures had peaked and declined as the soil containing the sensors approached the retaining wall, thinned, and began to spill over.

The divergence of subsurface tilts from

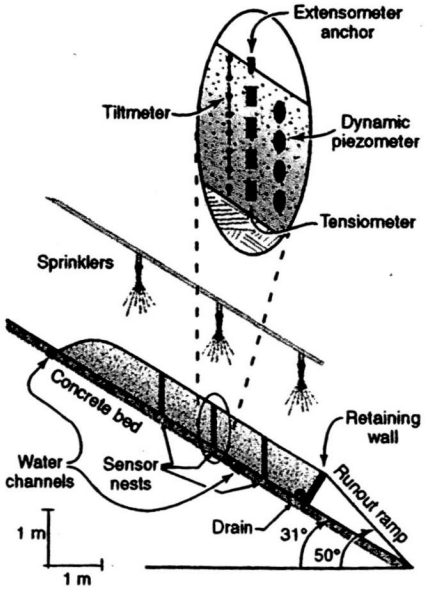

Fig. 1. Schematic longitudinal cross section of landslide experiments conducted at the U.S. Geological Survey debris flow flume, Oregon. The magnified ellipse depicts the positioning of sensors in vertical nests.

Fig. 2. Behavior of the loamy sand (Table 1) in a loose state (initial porosity 0.46) and dense state (initial porosity 0.41) when subjected to deformation in a ring-shear device (*23*). The device imposed shear displacements at 2 cm/s under constant normal loads of 10 kPa and permitted free drainage of water from the top and bottom of 7-cm-thick saturated soil specimens. Under these conditions, measured shear stress is a surrogate for effective soil strength. Loose soil (**A**) contracted monotonically during shearing, resulting in decreased porosity, transiently elevated pore pressure, and no peak in effective strength. Dense soil (**B**) initially dilated during shearing, resulting in increased porosity, transiently reduced pore pressure, and a prominent peak in effective strength. The porosity of the dense soil subsequently declined in response to breakage of soil aggregates (*24*). Triaxial unloading tests using a protocol described in (*7*) also produced contractive behavior for porosity 0.46 and dilative behavior for porosity 0.41.

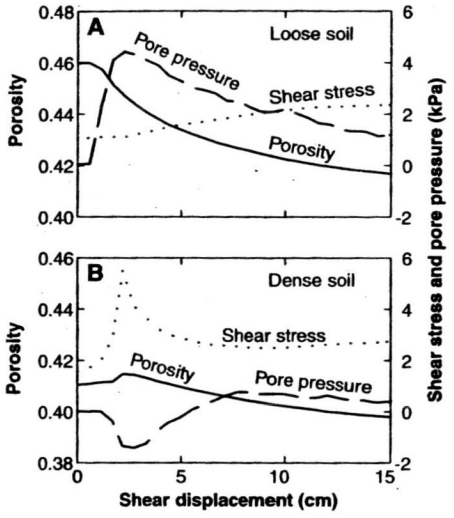

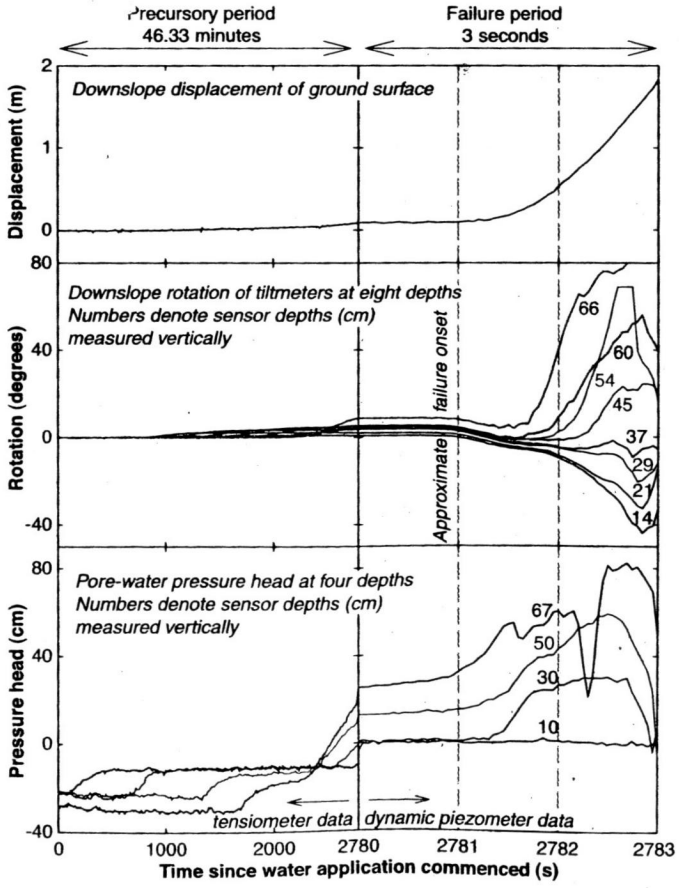

Fig. 3. Data recorded in a landslide experiment with loose soil (initial porosity 0.52 ± 0.02). To reveal details of behavior during the 3-s failure period, the time axis is expanded 927 times. All sensors were initially positioned 2.3 m upslope from the retaining wall (ellipse in Fig. 1). Different sensors measured pore water pressure heads in the precursory and failure periods (*17*).

2781.5 to 2782.5 s (Fig. 3) provides clues to the kinematics of slope failure. During the previous 1 s, tiltmeters at all depths rotated slightly upslope (negative tilts), but at around 2781.5 s, tiltmeters at depths ≥45 cm began to rotate rapidly downslope. This change in rotation coincided with a rapid increase in downslope landslide translation and likely resulted from drag due to sliding along the concrete bed. At the same time, accelerated upslope rotation above a depth of 45 cm provided evidence of superincumbent rotational landsliding. Despite this complex failure geometry, pore pressure responses at all depths indicated a relatively consistent pattern of soil contraction, which enhanced landslide acceleration.

Data from the experiment with dense soil (Fig. 4) imply a failure geometry similar to that of the loose soil but reveal markedly different landslide dynamics. Precursory pore water pressures necessary to trigger failure of the dense soil developed relatively slowly [owing to relatively low hydraulic conductivity (Table 1)], and were roughly twice as large as the pore pressures necessary to trigger failure of the loose soil [owing to high peak strength of the dense soil (Table 1 and Fig. 2)]. On average, motion of the landslide with dense soil proceeded about 300 times more slowly than motion of the landslide with loose soil (compare Figs. 3 and 4).

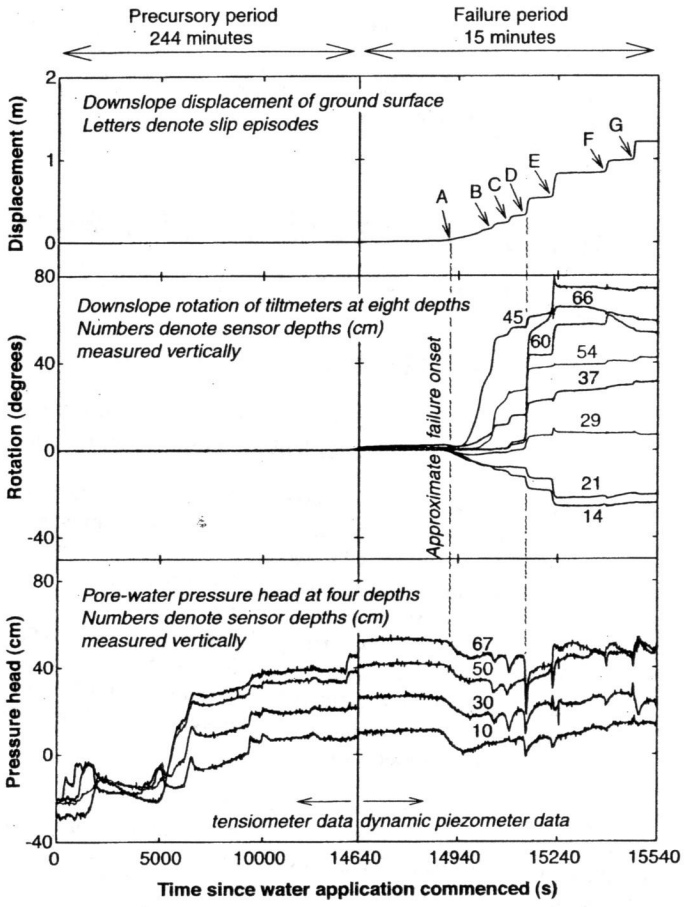

Fig. 4. Data recorded in a landslide experiment with dense soil (initial porosity 0.41 ± 0.01). To reveal details of behavior during the 15-min failure period, the time axis is expanded 16 times. All sensors were initially positioned 2.3 m upslope from the retaining wall (ellipse in Fig. 1). Different sensors measured pore water pressure heads in the precursory and failure periods (*17*).

Failure of the dense soil occurred episodically. At about 14600 s (Fig. 4), visible surface cracks and subsurface tilts of several degrees began to develop. At about 14,880 s (episode A in Fig. 4), visible landslide motion and soil dilation gradually commenced, with a consequent ~10-cm decline in pore water pressure heads. This initial episode of slow motion lasted >100 s but produced <0.2 m of downslope surface displacement. Subsurface tilts during this episode exhibited the same divergence as in the loose soil experiment; deep tiltmeters rotated downslope as the basal soil began to translate, whereas tiltmeters near the surface rotated upslope as superincumbent soil failed rotationally.

Subsequent slip episodes (B through G in Fig. 4) were similar to episode A but were somewhat briefer. Each episode was triggered when pore water pressures recovered sufficiently from the previous episode's dilation to help instigate renewed landslide motion. Most episodes involved concurrent pulses of surface displacement, subsurface tilt, and pore pressure decline. Downslope displacements during all episodes were <0.3 m and occurred at rates <0.1 m/s. Slip episode D (Fig. 4) caused a particularly prominent decline in pore pressure that reduced pressure heads by over 50% near the landslide base. Later slip episodes caused smaller pore pressure declines and in some instances a local pore pressure increase. Nonetheless, soil dilation continued to retard landslide motion, and soil porosity did not reach a homogeneous critical state even after displacements exceeded 1 m.

Although several factors in addition to initial porosity might influence landslide rates, in many instances these factors are either obvious [such as inertia (*21*)] or insignificant [such as intrinsic rate dependence of soil strength (*22*)]. In contrast, the dependence of landslide rates on soil porosity is not readily observable but can be pivotal. The dependence arises from the coupling of porosity change and pore pressure change, and it exists even if soil strength is otherwise constant.

The magnitude of pore pressure change induced by porosity change during landslid-

Table 1. Mean physical properties of loamy sand used in landslide experiments. *N* denotes the number of samples on which measurements were made in each experiment or soil test, and ± values indicate 1 SD from the mean.

Property (method or definition)	Loose soil experiment	Dense soil experiment
Mean texture (weight %) (wet sieving and sedigraph)	89% sand, 6% silt, 5% clay (N = 8)	89% sand, 6% silt, 5% clay (N = 8)
Initial moist bulk density (g/cm^3) [excavation method (*15*)]	1.44 ± 0.06 (N = 6)	1.82 ± 0.03 (N = 6)
Initial water content (water mass/solid mass)	0.12 ± 0.005 (N = 6)	0.14 ± 0.007 (N = 6)
Initial porosity (1 − dry bulk density/2.7)	0.52 ± 0.02 (N = 6)	0.41 ± 0.01 (N = 6)
Hydraulic conductivity (cm/s) (permeameter tests*)	0.025 ± 0.007 (N = 3)	0.0022 ± 0.00005 (N = 3)
Hydraulic diffusivity (cm^2/s) (drained compression tests*)	11 ± 4 (N = 2)	28 ± 6 (N = 2)
Friction angle at failure (degrees) (triaxial unloading tests*)	29 ± 2 (N = 2)	41 ± 1 (N = 2)

*These tests were conducted on reconstituted soil compacted to the desired porosity.

ing depends not only on initial porosity but also on the relative time scales for soil deformation and pore pressure diffusion (*18*). If fluid pressure can diffuse into or away from contracting or dilating soil as quickly as the soil deforms, pressure equilibration keeps pace with deformation and the effects of porosity change diminish. However, the time scale for pore pressure diffusion is h^2/D, where h is the typical thickness of the deforming soil mass and D is its typical hydraulic diffusivity. Even sandy soils with high diffusivity commonly have $D < 100$ cm^2/s (Table 1). Thus, the time scale for diffusive pore pressure equilibration in deforming soil masses with $h \sim 1$ m typically surpasses 10 s. In comparison, the time scale for landslide acceleration in response to basal pore-pressure change is $\sqrt{h/g}$ (*21*), which yields values <1 s for $h \sim 1$ m. We conclude that pore pressure diffusion can seldom keep pace with soil deformation and that relatively small variations in porosity can influence landslide behavior profoundly.

References and Notes

1. A. K. Turner, R. L. Schuster, Eds., *Landslides Investigation and Mitigation* (National Academy Press, Washington, DC, 1996).
2. Soil porosity (pore volume/total soil volume) ranges naturally from about 0.3 to 0.7 as a result of geological and biological modification of parent sediment or bedrock. An alternative measure of pore space is void ratio (pore volume/soil solids volume). Critical-state porosity depends not only on the physical properties of soil but also on the ambient state of stress and stress history.
3. A. Casagrande, *J. Boston Soc. Civ. Eng.* **1936**, 13 (January 1936).
4. A. N. Schofield, C. P. Wroth, *Critical State Soil Mechanics* (McGraw-Hill, New York, 1968).
5. G. Castro, thesis, Harvard University (1969).
6. R. W. Fleming, S. D. Ellen, M. A. Algus, *Eng. Geol.* **27**, 201 (1989).
7. S. A. Anderson, M. F. Reimer, *J. Geotech. Eng.* **121**, 216 (1995).
8. O. Reynolds, *Nature* **33**, 429 (1886).
9. On the scale of individual grains and pores, the coupling of fluid pressure and displacement of adjacent solids is described by viscous lubrication theory. On a continuum scale involving millions of grains and pores, the same coupling can be described by porosity change and attendant development and diffusion of pore fluid pressure.
10. Soil strength typically obeys the Coulomb-Terzaghi equation $\tau = (\sigma - p)\tan\varphi + c$, where τ is mobilized shear strength, σ is total normal stress, and p is pore fluid pressure, all on the same failure plane; φ is the soil angle of internal friction; and c is soil cohesion. Increased pore fluid pressure therefore reduces soil strength if all other factors are constant.
11. R. M. Iverson, R. G. LaHusen, *Science* **246**, 769 (1989).
12. D. Eckersley, *Geotechnique* **40**, 489 (1990).
13. G. Wang, K. Sassa, in *Environmental Forest Science* (Kluwer, Dordrecht, Netherlands, 1998), pp. 591–598.
14. All compaction loads were applied normal to the slope. The longest compaction periods produced the lowest porosities, and vibratory compaction produced more uniform porosities than did foot traffic.
15. G. R. Blake, in *Methods of Soil Analysis*, C. A. Black, D. D. Evans, J. L. White, L. E. Ensminger, P. E. Clark, Eds. (American Society of Agronomy, Madison, WI, 1965), pp. 374–390.
16. Tiltmeters were Crossbow model CXTA01-CAN, rigidly mounted in smooth cylindrical tubes 2.5 cm in diameter, fitted with rough exterior vanes 1 cm high to provide good frictional contact with soil. Extensometers were Celesco model PT101-250AS, attached to anchors embedded in the soil surface. Any use of trade, product, or firm names in this publication is for descriptive purposes only and does not imply endorsement by the U.S. government.
17. Dynamic piezometers were fabricated to have a configuration that promoted rapid dynamic response and minimal signal attenuation (*11*). The sensing elements in these piezometers were Honeywell Microswitch differential pressure transducers (model 26PCCFA3D, with nominal range 0 to 15 psi). Identical pressure transducers mounted to the pressure ports of Soil Moisture Equipment Jet-Fill tensiometers (model 2725, equipped with porous ceramic tips with nominal 1-bar air entry pressures) were used to measure pore water pressures less than atmospheric.
18. R. M. Iverson, M. E. Reid, R. G. LaHusen, *Annu. Rev. Earth Planet. Sci.* **25**, 85 (1997).
19. M. E. Reid, R. G. LaHusen, R. M. Iverson, in *Proceedings of the First International Conference on Debris-flow Hazards Mitigation*, C. L. Chen, Ed. (American Society of Civil Engineers, New York, 1997), pp. 1–11.
20. As illustrated in Fig. 2, dense soils generally display a prominent peak in strength (due to dilation), which impedes landslide initiation. After peaking, the strength of dense soils gradually decays. With sufficiently large deformations, dense soils and loose soils hypothetically approach a state of constant porosity (the critical state) and constant (residual) strength. Breakage of soil aggregates complicated this behavior in our ring-shear experiments (Fig. 2).
21. R. M. Iverson, *Water Resour. Res.* **36**, 1897 (2000).
22. S. Leroueil, M. E. S. Marques, in *Measuring and Modeling Time Dependent Soil Behavior*, T. C. Sheahan, V. N. Kaliakan, Eds. (American Society of Civil Engineers, New York, 1996), pp. 1–60.
23. N. R. Iverson, R. W. Baker, T. S. Hooyer, *Quat. Sci. Rev.* **16**, 1057 (1997).
24. J. E. Mann, N. R. Iverson, R. M. Iverson, *Eos (Fall Suppl.)* **80**, F443 (1999).

25. Supported in part by grant EAR9803991 from NSF. We thank K. Swinford for assistance with experiments and S. Ellen, J. Roering, and B. Muhunthan for critiquing the manuscript.

7 July 2000; accepted 14 September 2000

Rapid Evolution of Reproductive Isolation in the Wild: Evidence from Introduced Salmon

Andrew P. Hendry,[1]* John K. Wenburg,[2] Paul Bentzen,[2,3] Eric C. Volk,[4] Thomas P. Quinn[3]

Colonization of new environments should promote rapid speciation as a by-product of adaptation to divergent selective regimes. Although this process of ecological speciation is known to have occurred over millennia or centuries, nothing is known about how quickly reproductive isolation actually evolves when new environments are first colonized. Using DNA microsatellites, population-specific natural tags, and phenotypic variation, we tested for reproductive isolation between two adjacent salmon populations of a common ancestry that colonized divergent reproductive environments (a river and a lake beach). We found evidence for the evolution of reproductive isolation after fewer than 13 generations.

Ecological speciation occurs when organisms exposed to divergent selective regimes evolve reproductive isolation as a by-product of adaptation (*1–3*). Mechanisms contributing to ecological speciation include mate choice based on traits under divergent selection (*4*, *5*), hybrid or backcross inferiority (*2*), and reinforcement of assortative mating when hybrids are inferior (*6*, *7*). Ecological speciation appears to be relevant in allopatry and sympatry and has been supported by theoretical models, laboratory experiments, and studies of natural systems (*1–9*). Here we focus on an unknown aspect of ecological speciation: How quickly can reproductive isolation evolve?

Rapid evolution of adaptive traits often occurs in populations exposed to divergent ecological environments (*10*, *11*). Although this implies that reproductive isolation may also evolve rapidly, the best examples of ecological speciation are seen in groups that began diverging thousands of years ago (*12*, *13*). Unfortunately, inferring evolutionary rates on the basis of long-standing groups is questionable, because averaging disparate rates across time will obscure biologically important short-term evolution (*11*). Thus, reproductive isolation might evolve in only a few generations, or it may require a long and gradual accumulation of isolating mechanisms. Some insects that colonized new host plants 100 to 200 years ago have evolved ecologically mediated reproductive isolation (*14*, *15*). We ask whether reproductive isolation can evolve even faster by testing for evidence of intrinsic barriers to gene flow between two populations of sockeye salm-

[1]Organismic and Evolutionary Biology Program, University of Massachusetts, Amherst, MA 01003–5810, USA. [2]Marine Molecular Biotechnology Laboratory, University of Washington, 3707 Brooklyn Avenue Northeast, Seattle, WA 98105–6715, USA. [3]School of Aquatic and Fishery Sciences, University of Washington, Box 355020, Seattle, WA 98195, USA. [4]Washington Department of Fish and Wildlife, 600 Capitol Way North, Olympia, WA 98501, USA.

*To whom correspondence should be addressed. E-mail: ahendry@bio.umass.edu